האיגוד הישראלי למכניקה עיונית ושימושית

The Israel Society for Theoretical and Applied Mechanics (ISTAM)

http://istam.technion.ac.il

ISTAM-2006

"Material properties and failure at different scales"

1 January 2006

Tel Aviv University

ISTAM Annual Meeting
"Material properties and failure at different scales"

1 January 2006

Tel Aviv University

Table of Contents

ISTAM Annual Meeting
"Material properties and failure at different scales"

1 January 2006

Technical Program

Location: Rosenblatt Auditorium, Computer and Software Engineering Building, Tel Aviv University

09:30 – 09:50	Registration and coffee
09:50 – 10:00	*Opening:* M.B. Rubin, Technion, President of ISTAM
	<u>*Morning Session*</u> *Chairman:* M. Perl, Ben Gurion University
10:00 – 10:25	R. Segev, Ben Gurion University, *Notes on generalized stress concentration factors and optimal stress fields*
10:25 – 10:50	S. Ryvkin, Tel Aviv University, *Crack Approaching Bimaterial Interface*
10:50 – 11:15	J. Perry, Ben Gurion University, *An experimental-numerical model for the prediction of the three-dimensional residual stress field due to swage autofrettage*
11:15 – 11:40	Z. Yosibash, Ben Gurion University, *Edge singular solutions and extraction of edge stress intensity functions by p-FEM*
11:40 – 11:55	D. Elata, Technion, *Poster session overview*
11:55 – 13:00	*Graduate student poster session:* T.C. Gasser, I. Hariton, D. Klepach, V. Leus, R. Mahameed, Y. Motola, E. Priel, L. Shemesh, E.A. Socolsky, L. Tevet-Deree
13:00 – 14:00	Lunch (The registration fee includes lunch)
	<u>*Afternoon Session*</u> *Chairman:* I. Harari, Tel Aviv University
14:00 – 14:25	H.D. Wagner, Weizmann Institute of Science, *Adhesion of a living cell to a substrate: A model inspired by composite mechanics*
14:25 – 14:50	A. Zemel, Weizmann Institute of Science, *Cell interactions and polarization in elastic stress fields*
14:50 – 15:15	D. Shilo, Technion, *Nanoscale modulus mapping for high resolution measurement of the elastic modulus*
15:15 – 15:40	S. Givli, Technion, *Non-classical moduli for improved solutions of heterogeneous structures*

The annual membership fee to ISTAM is 50 NIS. It includes the lunch at the symposium and can be paid during the registration.

All lectures are open to the public free of charge

Notes on generalized stress concentration factors and optimal stress fields

Reuven Segev

Department of Mechanical Engineering
Ben-Gurion University
Beer-Sheva 84105, Israel. Email: rsegev@bgu.ac.il URL: http://www.bgu.ac.il/~rsegev

Traditional stress concentration factors specify the ratio between the maximal value of a stress component in a body and the maximum value of that component for simplified, idealized geometry. The stress concentration factors are evaluated using analytical, numerical and experimental methods for given loadings and material properties. It is noted that the nominal stress calculated for the simplified geometry may be regarded as the boundary traction at a large distance away from the nontrivial geometry. For example, for a finite plate containing a hole, the nominal stress may be regarded as the boundary traction on the edge of the plate. This suggests that the stress concentration factor be represented by the ratio

$$K_t = \frac{\sup_{x,i,k}\{|\sigma_{ik}(x)|\}}{\sup_{i,y}\{|t_i(y)|\}},\; x \in B,\; y \in \partial B\,,$$

where t is the surface force field defined on the boundary ∂B of the body. It is assumed throughout that the body is an open set in $\mathbb{R}^3$ having a differentiable boundary. In the last expression, the maximum over i in the denominator and the maximum over i,k in the numerator serve as norms on $\mathbb{R}^3$ and on the space $L(\mathbb{R}^3,\mathbb{R}^3)$ of linear mappings defined on $\mathbb{R}^3$. These may be replaced by other norms and we will use $|t(y)|$ to denote the norms of the values at $y \in \partial B$ of the surface force vector field. We denote by $|\sigma(x)|$ the norm of the the value of the stress at $x \in B$. Thus, the stress concentration factor may be written as

$$K_t = \frac{\sup_x\{|\sigma(x)|\}}{\sup_y\{|t(y)|\}},\; x \in B,\; y \in \partial B\,.$$

We ignore high values of the stresses if they are restricted to subsets of the body of zero volume. Similarly, we ignore high values of the surface force if it is restricted to subsets of the boundary of zero area. Thus, the suprema over x and y are in effect essential suprema. The concept of stress concentration is developed below in a number of steps. Firstly, we consider for the given external boundary loading t, the collection Σ_t of all stress fields that are in equilibrium with t. Thus, for $\sigma \in \Sigma_t$ we have

$$\int_B \sigma_{ik} w_{i,k}\, dV = \int_{\partial B} t_i w_i\, dA\,,$$

for any vector field w defined on the body. We denote by $K_{t,opt}$ the smallest stress concentration factor where we consider all stress fields σ in equilibrium with the given traction t. This may be conceived as a process of structural optimization. Thus,

$$K_{t,opt} = \inf_{\sigma\in\Sigma_t} \frac{\sup_x\{|\sigma(x)|\}}{\sup_y\{|t(y)|\}},\; x \in B,\; y \in \partial B\,.$$

Next, we arrive at a purely geometric property of the body. Noting that one usually does not know the exact nature of the loading in advance, we allow the force distribution to vary and consider the worst case, i.e.,

$$K = \sup_t\left\{K_{t,opt}\right\} = \sup_t\left\{\inf_{\sigma\in\Sigma_t} \frac{\sup_x\{|\sigma(x)|\}}{\sup_y\{|t(y)|\}}\right\}.$$

We refer to K as the *generalized stress concentration factor*. Clearly, the generalized stress concentration factor is a pure geometric property of the body.

Generalized stress concentration factors were considered in Segev [2003] and in Segev [2004]. In these works, the generalized stress concentration factor as defined above and related similar objects are shown to be identical to the norms of various trace mappings. We recall that the trace mapping γ extends consistently a function ϕ from the interior of a set Ω to a function $\gamma(\phi)$ defined on its boundary $\partial\Omega$. The norm of γ bounds the ratio between the L^1-norm of $\gamma(\phi)$ and the norm of ϕ. We will consider the mechanical relevance and properties of bounds on the trace mappings defined on the Sobolev space W_1^1, the space LD of integrable deformations (see Temam [1983]), and the quotient space LD/R, where R is the finite dimensional vector space of rigid vector fields.

A similar problem one might pose is the following. For a given traction field t, let $\sigma_{\max} = \max_x |\sigma(x)|$ be the maximal magnitude of the stress. Then, considering all the stress fields in equilibrium with t, find the lowest value S_t of $\sigma_{\max}$, i.e.,

$$S_t = \min_{\sigma\in\Sigma_t}\{S_t\} .$$

Noting that the calculation of the optimal maximal stress S_t from its definition is very difficult, the following expression is shown to hold

$$S_t = \max \frac{\left| \int_{\partial\Omega} t \cdot w \, dA \right|}{\int_{\Omega} |\varepsilon(w)| \, dV} .$$

References

Segev, R. (2003), “Generalized stress concentration factors”, *Mathematics and Mechanics of Solids,* to appear.

Segev, R. (2004), “Generalized stress concentration factors for equilibrated forces and stresses”, *Jounral of Elasticity,* accepted for publication.

Temam, R. (1983), *Problemes Mathematique sen Plasticite*, Bordas, Paris

Crack Approaching Bimaterial Interface

Shmuel Ryvkin[1*], Boris Nuller[2] and Alexander Chudnovsky[3]

(1) School of Mechanical Engineering, Tel Aviv University,
(2) Department of Applied Mathematics, Kirov Academy of Wood Technology, St. Petersburg
(3) Department of Civil and Materials Engineering, The University of Illinois at Chicago

Due to apparent practical implications, determination of the stress field in vicinity of the crack tip, approaching a bimaterial interface, has been addressed by many authors. As a rule, the result is obtained from the numerical solution of singular integral equation. However, the switch of the singularity type in the near tip stress asymptotic from $r^{-1/2}$ for the crack fully imbedded in one of the materials to the $r^{-\lambda}$, $0<\lambda<1$ for the crack impinging on an interface does not allow to carry out an accurate numerical investigation of the phenomenon and predict the type(stable/instable) of the crack propagation.

The suggested approach is based on the closed form solution obtained by the Wiener-Hopf method. The problem on a Green function for a semi-infinite Mode I crack perpendicular to the interface between two dissimilar elastic half planes is considered. The distance ε between the crack tip and the interface is served as a length scale of the problem. After the factorization and the expansion of the inverse transform integrals into the residue series one obtains a simple formulas for the stresses and stress intensity factor (SIF). The latter is expressed in the form $K_I=\varepsilon^{p1-1/2} f(\alpha,\beta)$, where α and β are the Dundurs elastic mismatch parameters and p_1 is the first root of Zak-Williams characteristic equation for the auxiliary problem on a crack terminating at the interface. Consequently, the stability of the crack behavior is directly derived from the fact whether p_1 is more or less than 1/2. A new parameter of the interface, χ, is introduced to characterize the crack stability. This parameter is a simple combination of shear moduli G_i and Poisson's ratios ν_i of materials on both sides of the interface

$$\chi = \frac{G_1\kappa_2}{G_2\kappa_1}, \qquad \kappa_i = 3-4\nu_i, \qquad i=1,2.$$

Crack stability and instability regions in the α,β plane are shown in the Figure. The dashed line corresponds to the equal moduli of the materials on both sides of the interface.

In the case of a stable crack the SIF vanishes when $\varepsilon\to 0$ the standard approach of the linear elastic fracture mechanics becomes inapplicable. Therefore one have to consider the complete stress distribution in front of the crack which is readily provided by the obtained solution.

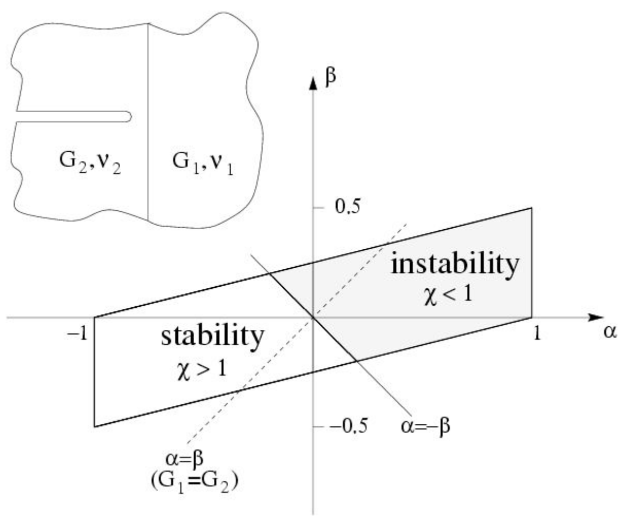

An Experimental-Numerical Model for the Prediction of the Three-Dimensional Residual Stress Field Due to Swage Autofrettage

M. Perl and J. Perry*
Pearlstone Center for Aeronautical Engineering Studies
Department of Mechanical Engineering
Ben-Gurion University of the Negev
Beer-Sheva 84105, Israel

The optimal design of gun barrels has two major goals: (a) to increase the strength to weight ratio of the barrel and (b) to prolong the barrel's total fatigue life. Both goals can be simultaneously achieved by introducing a favorable residual stress field, through the barrel's wall, commonly by the autofrettage process. Presently, there are two distinct processes for overstraining the gun tube: hydrostatic autofrettage or swage autofrettage.

Several theoretical solutions for the residual stress field due to hydrostatic autofrettage, based on Lamé's solution and vonMises or Tresca yield condition, are presently available. Furthermore, in recent years the Bauschinger effect was introduced into these models, yielding very realistic results. Though several attempts have been made to model swage autofrettage, none of them reasonably reproduces the actual process nor do they predict any of the experimental results.

The residual stress field due to hydrostatic autofrettage is usually assumed to be a two-dimensional axisymmetric stress field. This stress field is commonly solved in terms of the radial displacement U (U_r) that solely depends on the radial coordinate r. In the case of swage autofrettage the residual stress field needs to be modeled as an axisymmetric 3-D stress field. Such a model includes the radial and the axial displacements U (U_r) and W (U_z), both depending on the radial and the axial coordinates i.e., r and z respectively.

The present analysis suggests a new three-dimensional numerical model for evaluating the residual stress field due to swage autofrettage. This procedure is based on the idea of solving the elasto-plastic problem using the form of elastic solution. In the compatibility equations and in Hooke's law the elastic strains are replaced by the difference between the total and plastic strains. These new equations are introduced in to the general axisymetric equilibrium equations, which are then approximated by finite differences. The finite difference equations are solved using the Gauss-Seidel iterative procedure.

During loading and unloading isotropic hardening is introduced, using experimental uniaxial tension or compression stress-strain curves. The kinematic hardening is taken into account using the Bauschinger Effect Factor (BEF) curve, obtained from uniaxial tension-compression cycling tests.

The force required to move the oversized mandrel forward is calculated using the concept of a cylinder and rod shrink-fit. For each pressure increment, the displacement increment is calculated. Multiplying the length increments by the mandrel's diameter and the friction coefficient, results in a force increment. The total force is determined by integrating the force increment up to the maximal pressure .

In order to validate the numerical results, a full-scale experiment was conducted on a standard swage autofrettage industrial machine, which was instrumented accordingly. Strain gauges were attached to both the barrel and the mandrel's rod, in order to monitor the pushing force and the radial and the axial strains.

The present 3-D numerical model is found to simulate the actual process of swage autofrettage and to predict the experimental findings very well. The calculated maximal strains, residual strains, the Permanent Bore Enlargement (PBE) as well as the mandrel pushing force were found to be in very good agreement with the measured values.

Once a 3-D solution of the residual stress field is obtained it can be used not only for swage autofrettage calculations but also for three-dimensional crack analysis and for the estimation the barrel's fatigue life.

Edge singular solutions and extraction of edge stress intensity functions by p-fem1

Zohar Yosibash* and Netta Omer
Computational Mechanics Lab., Dept. of Mechanical Engineering
Ben-Gurion University
Beer-Sheva, Israel 84105
zohary@bgu.ac.il

The asymptotic solution of elasticity problems, in the vicinity of edges in 3-D domains is provided explicitly. It involves a sequence of eigen-pairs and their corresponding coefficients which are functions along the edge. The determination of these eigenpairs (and more importantly their shadows), and reliable computation of the coefficients (edge stress intensity functions) of the asymptotic expansion will be addressed in this talk. These are of practical engineering importance because failure theories involve them.

Recent results, on the special structure of edge-singularities, including so-called shadow eigen-functions, will be presented [1]. New methods for the computation of their characteristics will be demonstrated by numerical methods: namely the quasi-dual method for the computation of the edge stress intensity functions. These are used in conjunction with the p-FEM and numerical examples will be provided including the Compact Tension Specimen frequently used for the determination of toughness [2][3].

References

[1] Costabel M., Dauge, M. and Yosibash Z., "A quasidual function method for extracting edge stress intensity functions", SIAM Journal on Mathematical Analysis, 35, No. 5, (2004), pp. 1177-1202.
[2] Omer N., Yosibash Z., Costabel M. and Dauge, M., "Edge Flux Intensity Functions in Polyhedral Domains and their Extraction by a Quasidual Function Method", International Journal on Fracture,129, (2004), pp. 97-130.
[3] Yosibash Z., Omer N., Costabel M. and Dauge, M., "Edge Stress Intensity Functions in Polyhedral Domains and their Extraction by a Quasidual Function Method", to appear in International Journal on Fracture.

Research performed in collaboration with Martin Costabel and Monique Dauge from Universit´e de Rennes 1, Rennes, France.

Adhesion of a living cell to a substrate
A model inspired by composite mechanics

D. Raz–Ben Aroush and H.D. Wagner*
Department of Materials & Interfaces, The Weizmann Institute of Science
Rehovot 76100, Israel

A shear-lag type mechanical model classically used in the field of composite material science is applied to the context of a cell adhering to a substrate through focal adhesion sites. An analogy indeed exists between the experiment that consists in pulling-out a stiff fiber from a soft matrix in order to measure their mutual adhesion, on the one hand, and the mechanosensing process that enables a cell to probe a substrate and generate a level of adhesion that is sufficient to achieve locomotion or other tasks, on the other.

Significant results emerge from this analogy. The full profile of shear stress along a focal adhesion can be calculated and the main result is the fact that the maximum shear stress occurs at the internal edge of the focal adhesion area, with likely biochemical implications on cell adhesion activity. Calculations show that focal adhesion growth leads to a significant decrease in shear stresses (Fig. 1). The effect of the material and geometrical parameters of the focal adhesion components and of the extracellular matrix, as well as questions pertaining to the entire cell morphology such as the extent of mechanical interactions between neighboring focal adhesions, are explored, using mechanics as a guide. Our results are expected to lead to further experimental work in new directions.

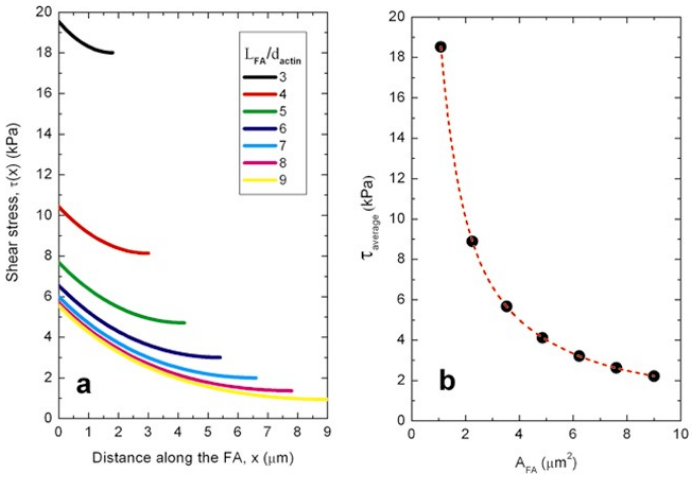

Fig. 1. (a) Shear stress profiles along the FA length, using pertinent aspect ratios. The origin of the x-axis (x=0) corresponds to the border between the actin filament and the FA area. Negative values of x correspond to positions within the actin filament, positive values to positions within the FA. (b) The average shear stress, $\tau_{average}$, versus the FA area.

Reference:

D. Raz-Ben Aroush and H.D. Wagner, "Adhesion of a living cell to a substrate - A model inspired by composite mechanics", Submitted (August 2005).

Cell interactions and polarization in elastic stress fields

Assaf Zemel*, Ilka Bischofs and S. A. Safran

Department of Materials and Interfaces, Weizmann Institute of Science
Rehovot 76100, Israel
Email: assaf.zemel@weizmann.ac.il

Many tissues of multicellular organisms are affected by the presence or absence of mechanical loads: gravitational compressive forces control the deposition of bone, isotonic tension causes muscles to grow, and normal hydrostatic pressure in blood vessels promote the maturation of vascular smooth muscle. Understanding the response of single cells in artificial substrates to mechanical loadings, and their behavior as a collective, may shed light on the processes that occur in a living tissue.

Individual cells possess specific mechanisms that enable them to sense and respond to changes in their mechanical environment. By pulling on their environment cells sense rigidity gradients, boundaries and strain. Many cell types respond to these signals by actively adjusting cell polarity. On a macroscopic level, the forces generated by a collection of cells in a tissue significantly alter the overall elastic response of the system.

We predict the response of cells in a three dimensional elastic medium to externally applied strain fields. The cells are modeled as polarizable elastic force dipoles that can change their orientation in response to the local elastic stress. We model the ensemble of cells by an extension of the treatment of dielectric response of polar molecules. We introduce the elastic analogy of the dielectric constant of the medium that allows us to predict the average cell polarization, their orientational order, and the effective material constants.

Nanoscale Modulus Mapping for High Resolution Measurement of Elastic Modulus

D. Shilo* and Y. Ganor

Department of Mechanical Engineering, Technion - Israel Institute of Technology
Haifa 32000, Israel, email: shilo@tx.technion.ac.il

The rapidly development in the field of nanotechnology increases the need for measuring a variety of material properties with a nanoscale spatial resolution. In particular, mapping of mechanical properties at the nanoscale is crucial for successful development of new thin films, composite materials, and nanoscale assemblies. Recently, a new modulus mapping technique has been developed, based on a nanoindentation instrument equipped with a piezo-scanner and dynamic force modulation electronics.

This work presents an optimization scheme of this technique, utilized to resolve between regions with close values of elastic moduli, which are typical to multiphase or multi-domain materials. For this purpose, we introduce a procedure for finding the experimental parameters that provide the best modulus contrast. The procedure is based on an analysis of the dynamic mechanical response of a system comprised of a nanoindentation transducer, a probing tip and the specimen. We applied the procedure on a ferroelectric $BaTiO_3$ single crystal. The obtained images show a clear contrast of a 90 degrees domain microstructure, i.e. regions that have the same material phase but different orientation of the tetragonal unit cell. The extracted reduced modulus values are in good agreement with both conventional nanoindentation measurements and reported bulk elastic moduli.

Non-Classical Moduli for Improved Solutions of Heterogeneous Structures

Sefi Givli

Faculty of Mechanical Engineering, Technion - Israel Institute of Technology
Haifa 32000, Israel. Email: mesefi@tx.technion.ac.il URL: http://tx.technion.ac.il/~mesefi/

Morphology related response of structures is important in many mechanical applications. In particular, the mechanical response of structures with dimensions in the same size order of their microstructure deviates significantly from the prediction based on effective properties. Examples are micro-scale structures used in MEMS devices, which are routinely manufactured from polycrystals and are comprised of very few grains, nanowires have a non-negligible substructure size, porous ceramics, bones, biological membranes and more.

The analysis of heterogeneous structures, with either stochastic or deterministic material properties, has been a major subject of research for more than three decades. Much effort has been devoted to implementing the randomness of the heterogeneity into Finite Element Method and Monte Carlo simulations. Analytical studies are mostly applied to very simple problems, and are usually solved by inverse problem approach or perturbation methods. In recent studies (e.g. Altus et. al, 2001, 2003, 2005), a Functional Perturbation Method (FPM) has been developed, which proposes a unified approach for the analysis of heterogeneous structures (stochastic or deterministic).

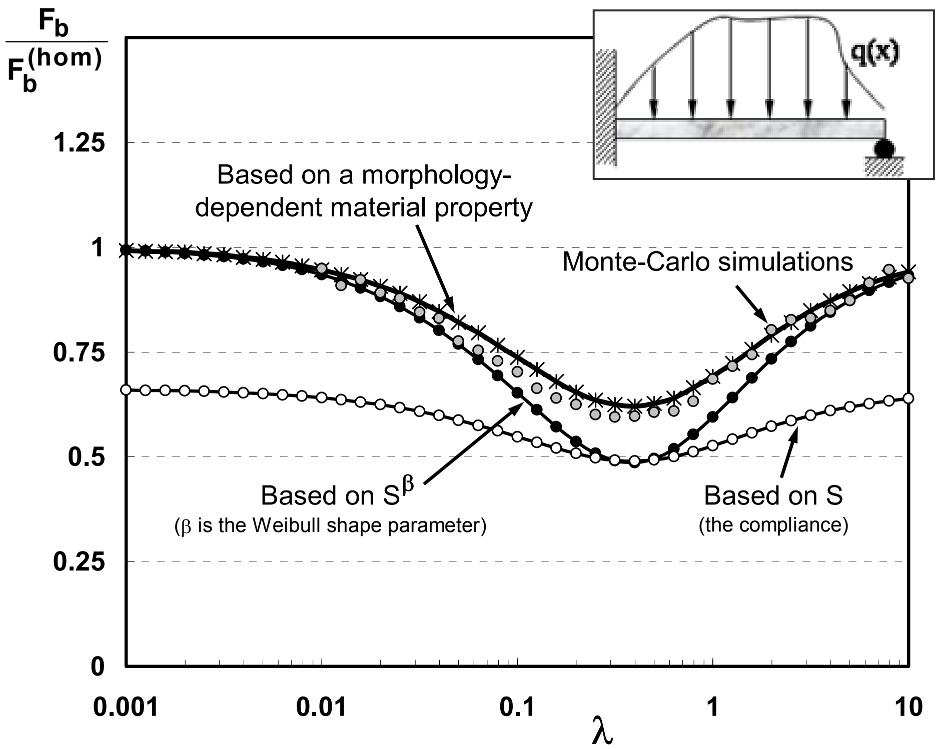

Figure 1: Failure probability of a statically indeterminate beam as a function of the morphological correlation length. The failure probability of the beam, limited to 2-points statistics, is calculated based on various material properties and compared to Monte-Carlo simulations.

The FPM is based on treating the response of the structure (e.g. deflections, buckling load, strength, stress-field etc.) as a *functional* of material heterogeneity (morphology). Then, the response is functionally expanded as a Fréchet series around an arbitrarily chosen material property. The accuracy of the solution is affected by three different sources of approximations: a.) Simplifying assumptions (for example, in beam deflection - Bernoulli, Timoshenko or any other high order theory), b.) The number of terms used in the functional perturbation series, and c.) The specific material property on which the FPM is applied. While the first two sources come from "common" accuracy related problems, which appear also in regular perturbation methods, the third involves functional differentiations and has not be addressed before. Thus, the third source is the prime subject of this study.

To demonstrate the importance of the subject, consider a 1D rod with a non-uniform (deterministic) stiffness E(x). The differential equation associated with the displacement, u(x), of the rod is

$$E_x u_{x,xx} + E_{x,x} u_{x,x} = q_x . \tag{1}$$

where q(x) is the distributed load exerted on the rod. For this problem, it is "natural" to execute a "regular" perturbation method associated with a perturbation on E. This approach leads to a solution composed of an infinite series (except for extremely simple functions of E), and its accuracy depends on the number of terms considered. On the other hand, it can be shown that by introducing the compliance (E^{-1}) into (1), the *exact* solution can be restored by a perturbation series involving two terms only.

In problems involving stochastic material properties, the solution is usually obtained as a series of increasing orders of point-correlations. In practice, only partial morphological information is available (commonly 1-point and 2-points statistics). We show that, under such limitations, introducing non-classical material properties into the analysis can significantly improve the accuracy of the solution. Moreover, these material properties are morphology-dependent. As an example, consider the failure probability of a statically indeterminate beam with stochastic bending stiffness, in which failure is attributed to the weakest link principle. The normalized failure probability, limited to the 2-points statistics, is illustrated in Fig.1 as a function of the morphological correlation length, and is compared to Monte-Carlo simulations. It is evident that the "morphology dependent" material property, suggested by this work, leads to significantly improved accuracy of the solution through the entire range of correlation lengths, and corresponds to the exact solution in the limit cases of very small or very large correlation lengths.

References:

Altus E., 2001, "Statistical Modeling of Heterogeneous Microbeams", Int. J. Solids and Structures, 38:5915-5934.

Givli S, Altus E, 2003, "Effect of modulus-strength correlation on the reliability of randomly heterogeneous beams", Int. J. Solids Structures 40(24):6703-6722.

Altus E., Totry E., Givli S., 2005, "Optimized Functional Perturbation Method and Morphology Based Effective Properties of Randomly Heterogeneous Beams", Int. J. Solids Structures 42:2345-2359.

Givli S, Altus E, 2005, "Improved Functional Perturbation Method for Reliability Analysis of Randomly Heterogeneous Beams", Structural Safety, in press.

Poster session

Stress-driven collagen fiber remodeling in arterial walls

I. Hariton[1*], G. deBotton[1], T. C. Gasser[2], G. A. Holzapfel[2,3]

[1] The Pearlstone Center for Aeronautical Studies,
Department of Mechanical Engineering,
Ben-Gurion University, Beer-Sheva 84105, Israel
[2] School of Engineering Sciences, Royal Institute of Technology,
Osquars backe 1, SE-100 44 Stockholm, Sweden
[3] Computational Biomechanics, Graz University of Technology,
Schiesstattgasse 14-B, A-8010 Graz, Austria

A stress-driven model for the relation between the collagen morphology and the loading conditions in arterial walls is proposed. We assume that the two families of collagen fibers in arterial walls are aligned along preferred directions, located between the directions of the two maximal principal stresses. For the determination of these directions an iterative finite element based procedure is developed. As an example the remodeling of a section of a human common carotid artery is simulated. We find that the predicted fiber morphology correlates well with experimental observations (Figure 1). Interesting outcomes of the model including local shear minimization and the possibility of axial compressions due to high blood pressure are revealed and discussed.

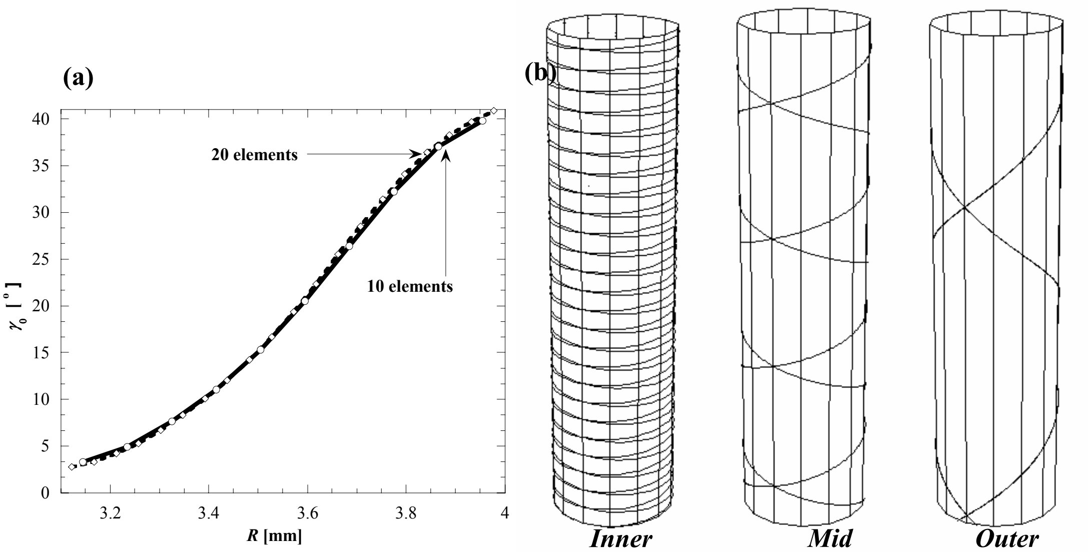

Fig. 1. (a) Variation of the fiber alignment angle γ_0 versus radial location R in the reference configuration. The continuous and dashed curves were determined with FE meshes consisting of 10 and 20 elements across the arterial wall, respectively. (b) The double-helix architecture of the collagen fibers at the inner, mid and outer radii of a common carotid is reproduced.

Reference:

I. Hariton, G. deBotton, T. C. Gasser, G. A. Holzapfel, "Stress-driven collagen fiber remodeling in arterial walls", Biomechanics and modeling in mechanobiology (submitted).

Postbuckling response and ultimate strength of a rectangular elastic plate using a 3-d Cosserat brick element

D. Klepach*, and M.B. Rubin

Faculty of Mechanical Engineering
Technion - Israel Institute of Technology
32000 Haifa, Israel
E-mail: mbrubin@tx.technion.ac.il

Use is made of a 3-D Cosserat brick element which admits full material and geometric nonlinearity to determine the postbuckling response of a rectangular plate and its ultimate strength. Examples are discussed which show that existing approximate solutions are more limited that originally anticipated.

Buckling of plates and shells has been a topic of great interest for a number of years. Although the determination of the bifurcation (onset of buckling) of plates is well known, for the postbuckling response the deformed shape must be treated as a curved shell even when the reference shape was a flat plate. Moreover, the nonlinear equations also include the influence of bending on the membrane stresses that are the primary cause for buckling. The main objective of this work is to analyze the postbuckling response of a square plate and the ultimate strength of a rectangular plate. Specifically, it is shown that the approximate analytical solutions discussed in Timoshenko and Gere [1] are more limited than originally anticipated and that the postbuckling process associated with the ultimate strength of the plate is different from that presumed in the simple analysis.

Here, attention is focused on an isotropic elastic rectangular plate with length L, width W and thickness H. The plate is modeled using 3-D Cosserat brick elements. It has 8 nodes with 24 degrees of freedom, it includes both material and geometric nonlinearities and it is invariant under superposed rigid body motions. The main difference between the Cosserat point approach and standard finite element formulations appears in the constitutive equations for the element. In the Cosserat approach these equations are hyperelastic with the intrinsic director couples being determined by algebraic equations in terms of derivatives of a strain energy function. In contrast with standard finite element formulations, the Cosserat approach needs no integration through the element region to determine the constitutive response.

Figure 1 plots results for compression with no lateral deformation of a square plate. The axial compressive force P and the axial compressive strain ε are normalized, respectively, by the force P_{cr} and strain ε_{cr} associated with bifurcation. Also, w_M is the displacement of the plate's midpoint normal to its reference surface. Figure 1a shows that the approximate analytical expression (TG) discussed in [1] is more limited than originally anticipated and Figure 1b indicates that the Cosserat solution (C) predicts an unexpected snap-through phenomena as the mode shape changes abruptly.

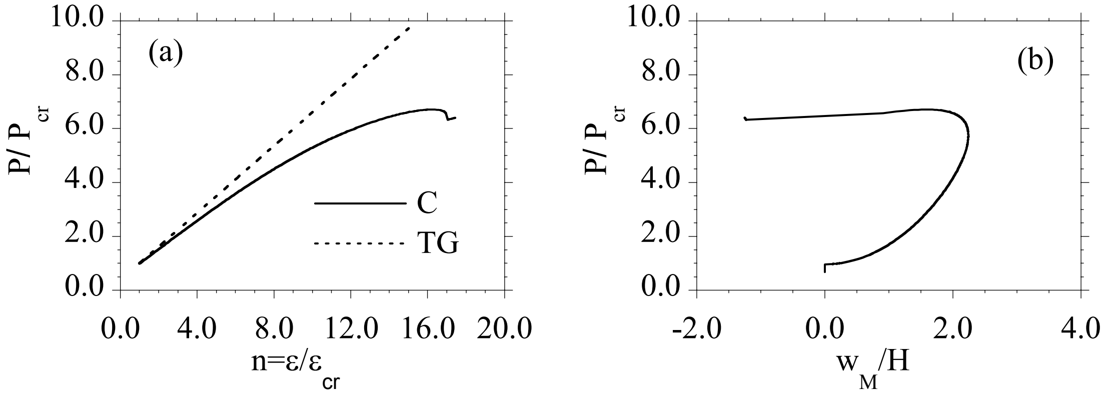

Figure 1. Compression with no lateral deformation. (a) predictions of the normalized force P / P_{cr} versus the normalized applied strain $n = \varepsilon / \varepsilon_{cr}$ for the approximate analytical expression (TG) and the Cosserat solution (C); and (b) numerical predictions of the postbuckling curve.

Figure 2 shows that as a rectangular plate is compressed in uniaxial stress the development of lateral tension causes the plate to divide into subdivisions which are rectangular instead of square, as predicted by the linearized theory. The ultimate strength of the plate occurs when the subdivision yields before the plate further subdivides elastically. This postbuckling process is different from that presumed in the simple analysis described in [1].

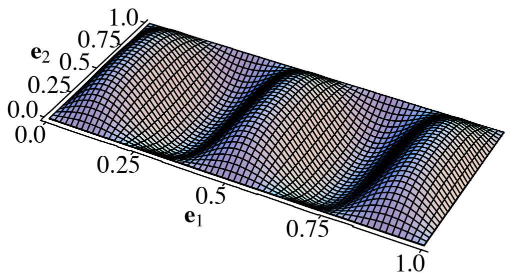

Figure 2. Uniaxial stress. A plate buckling into subdivisions which are rectangular instead of square.

Reference

[1] Timoshenko, S.P., Gere, J.M. (1961): Theory of elastic stability. McGraw-Hill, New York.

The dynamic response of voltage and charge driven electrostatic switches

V. Leus* and D. Elata

Technion - Israel Institute of Technology, Haifa 32000, Israel
Email: elata@tx.technion.ac.il, Phn: +(972) 4 8293184, FAX: (+972) 4 829 5711

Abstract: The un-damped dynamic response of charge-driven and voltage-driven electrostatic switches is analyzed. It is shown that charge actuation can drastically reduce the impact velocity between the switch electrodes and reduce unwanted vibrations during switch release. It is also shown that in capacitive switches, charge actuation considerably reduces the maximal electrostatic field within the dielectric layer.

INTRODUCTION

Electrostatic actuation is a prevalent method for driving Ohmic and capacitive RF-MEMS switches [1, 2]. Current electrostatic switches utilize the pull-in instability to rapidly switch between two states [3, 4]. Three parameters of the dynamic response of electrostatic switches are of special interest: the switching time, impact velocity, and the relaxation time during switch release.

Switching time can be reduced by increasing the actuation voltage, and by packaging the switch in vacuum to reduce damping. However, this will increase the impact velocity between the switch electrodes. High impact velocity may result in contact bouncing that extends the switching time [5], and may also affect the switch reliability (e.g. pitting damage [2]).

Contact bouncing can be reduced by using hermetic packaging with inert gas at low pressure, rather than a vacuum package [5]. The gas damping can also reduce the relaxation time in switch-release by attenuating unwanted vibrations. However, the same damping inevitably increases the switching time.

MODELING

In this study, we analyze the un-damped dynamic response of electrostatic actuators that are driven by a step-function of voltage or by a step-function of charge.

It is shown that by using charge actuation rather than voltage actuation, the impact velocity and release vibrations can be drastically reduced. Furthermore, it is shown that charge actuation can also reduce the electrostatic field across the dielectric layer in capacitive switches. This should reduce the dielectric charging that affects the switch response.

As a model problem of an electrostatic switch, we first consider the parallel-plates actuator illustrated in Fig. 1. The actuator is constructed from a top electrode of mass m and area A that is suspended on a linear elastic spring with stiffness k, above a fixed bottom electrode. The bottom electrode is coated with a dielectric layer of thickness d_0, and the initial gap between the top electrode and the dielectric is g. The fixed bottom electrode is electrically grounded and a voltage V or a charge Q may be applied to the top electrode.

The position and velocity of the movable electrode are derived for both charge and voltage actuation. Figures 2,3 present the position, velocity, voltage and charge, all as function of time, of a parallel-plates actuator (normalized values are presented). Fig. 2 presents the dynamic response under charge actuation, with voltage actuation for hold-down. Fig. 3 presents the dynamic response for the prevalent voltage actuation. In both figures the enforced charge (or voltage) is marked in solid lines, and the reactive voltage (or charge) is marked in dotted lines.

As shown, under charge actuation the impact velocity can be reduced to zero while under voltage actuation the impact velocity is considerable. Furthermore, under charge actuation the electric field in the dielectric layer is small and constant. This field is even lower than the electric field required for hold-down. In contrast, in voltage actuation the electric field in the dielectric layer rapidly increases with the progression of switching. The high field intensity under voltage actuation

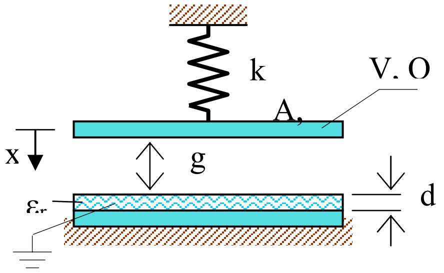

Figure 1. Schematic view of the parallel-plates actuator with a dielectric layer coating the bottom electrode.

may cause dielectric charging that can affect the electromechanical response of the system.

It is also shown that under charge actuation the switch can reach the open state ($\tilde{x}=0$) with zero velocity (e.g. $\dot{\tilde{x}}=0$). At this point, grounding the electrode (application of a zero voltage) will leave the movable electrode at the unloaded state. In contrast, under voltage actuation switch release is characterized by free vibrations.

In this study we show that the same features of the dynamic response are applicable to more realistic switches such as the clamped-clamped bridge over a co-planar wave-guide (Fig. 4).

REFERENCES

1. H.J. De Los Santos, *RF MEMS circuit design for wireless communications*. Boston: Artech House, 2002.
2. G.M. Rebeiz, *RF MEMS : theory, design, and technology*. Hoboken, N.J.: Wiley, 2003.
3. S.D. Senturia, *Microsystem design*. Boston: Kluwer Academic Publishers, 2001.
4. J.A. Pelesko and D. H. Bernstein, *Modeling MEMS and NEMS*. Boca Raton, FL: Chapman & Hall/CRC, 2003.
5. P.G. Steeneken et al., *JMM*, **15**, 176-184, 2005.

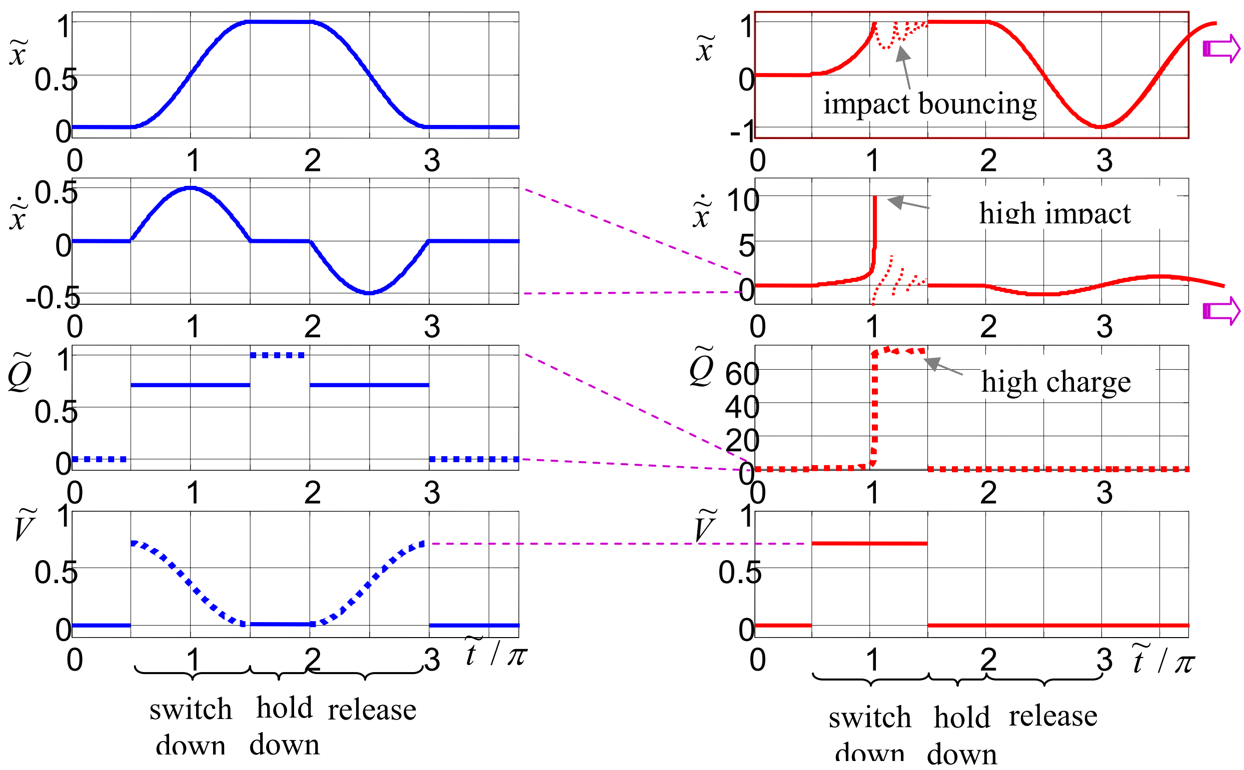

Legend: $\tilde{x}$ - position, $\dot{\tilde{x}}$ - velocity, $\tilde{Q}$ - charge, $\tilde{V}$ - voltage.

*Figure 2. Switching and release responses of the parallel-plates actuator under **charge actuation**. The applied electrostatic variable (charge or voltage) is marked by a solid line and the reactive variable (voltage or charge) is marked by a dotted line.*

*Figure 3. Switching and release responses of the parallel-plates actuator under **voltage actuation**. The contact bouncing is schematically illustrated to show that it extends the switching time. In the un-damped actuator, the switch release vibrations are not attenuated.*

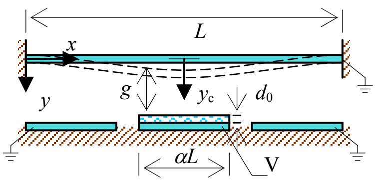

Figure 4a. A typical RF-MEMS shunt switch showing the clamped-clamped beam actuator The driving electrode is coated by a dielectric insulator

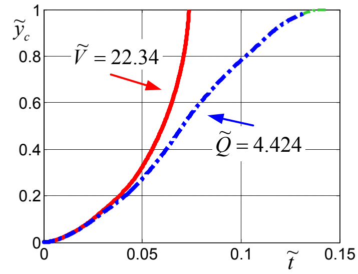

Figure 4b. Deflection of the c-c beam actuator for voltage (solid) and charge (dashed) actuation.

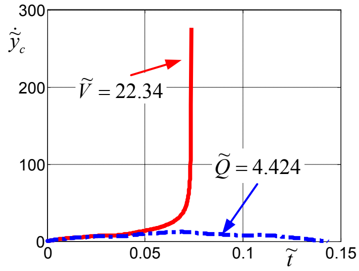

Figure 4c. Velocity of the c-c beam actuator for voltage (solid) and charge (dashed) actuation.

A Temperature-Gradient Driven Micromirror With Large Angles and High Frequencies

Rashed Mahameed* and David Elata
Faculty of Mechanical Engineering, Technion - Israel Institute of Technology
Haifa 32000, Israel. Email: mrashed@tx.technion.ac.il URL: http://mems.technion.ac.il/

In this work we demonstrate that thermoelastic actuation can be used to drive tilting micromirrors to *large angles* at *high frequencies*. We present a Single Crystalline Silicon (SCS) micromirror with 1 *mm* diameter that achieves a scanning deflection angle of ±8.5° at 9.5 *kHz*, which is driven by a 1.5 *Volt* source. The key feature that enables the high frequency of the thermoelastic actuator is that it uses temperature gradient as the driving force rather than using temperature itself as in prevalent thermoelastic actuators.

Micromirrors are used in laser machining, printers, scanners, laser surgery, optical switching communication networks, and more [1]. Different actuation methods have been used to drive micromirrors. These actuation methods include electrostatic, piezoelectric, electromagnetic and thermoelastic actuation. Electrostatic actuation is prevalent due to its compatibility with microfabrication technology but it requires relatively high voltages and may suffer from instabilities [2-3]. Piezoelectric and electromagnetic actuators require special materials and processes.

Thermoelastic actuation is also compatible with standard microfabrication technology but it is known to be rather slow [4]. To achieve large dynamic deflections using the existing thermoelastic actuation schemes, the entire actuator needs to be heated and cooled. Due to the large time required to achieve the actuation temperature, and the time required to cool the structure, the thermoelastic response is often too slow.

However, by using the temperature gradient as the driving force rather than temperature itself, the actuator response-time can be considerably reduced. The driving force in temperature-gradient actuation is the thermomechanical moments induced in the actuator beam. These moments develop primarily under a heater that is fixed to one side of the actuation beam while a heat sink is located on the opposite side of the beam. The temperature gradients fully develop within a time scale that is much shorter than the time required to heat or cool the entire structure. Therefore, the temperature-gradient actuation has a very shorter response time [5]. In this work the temperature-gradient actuation method is used to drive a scanning micromirror to a large deflection angle of ±8.5º at a high frequency of 9.5 *kHz*.

A schematic view of the temperature-gradient driven micromirror is presented in Fig. 1. The 1 *mm* diameter circular mirror is suspended on two flexible cantilever beams on each side. The suspension beams are clamped to a solid anchor (device frame) that serves as a heat sink. Resistive heaters supply a square waveform of heat over a confined region of the upper surface of the suspension beams, in the vicinity of the anchor. By supplying heat flux simultaneously to two beams on the same side of the torsion axis (blue or red electrode in Fig. 1), a bending moment develops in the beams edges. The supplied square waveforms V_1 and V_2 are in a 180º relative phase shift (Fig. 1). Due to the geometry of the device, these bending moments are translated to a torque that is applied on the mirror.

The micromirror device is machined from a 20μm thick layer of SCS using SOI technology and the resistors are sputtered metal serpentines (Fig. 2). The vertical deflection of the mirror was measured with a Polytec Laser Vibrometer. The device is packaged in vacuum with a pressure of 8×10^{-3}*mbar*. The FFT of the measured tilt angle (Fig. 3) shows that the time response is sinusoidal (Fig. 4). The frequency response for two values of the applied voltage is presented in Figs. 5 and 6. The nonlinear nature of the mirror response which is attributed to the stress stiffening [6] of the suspension beams, is apparent in these figures.

Reference:

[1] M. Kiang et al., JMEMS, 7(1), pp. 27-37, 1998.
[2] S. Ahn et al., JMM, 14, pp. 1455 - 1461, 2004.
[3] J. Singh et al., Sensor. Actuat. A, Article in press.
[4] S. Schweizer et al., Sensor. Actuat. A,76, pp. 470-477, 1999.
[5] R. Mahameed et al., JMM, 15, pp. 1414-1424, 2005.
[6] A.H. Nayfeh et al., Nonlinear Oscillations, John Wiley, 1979.

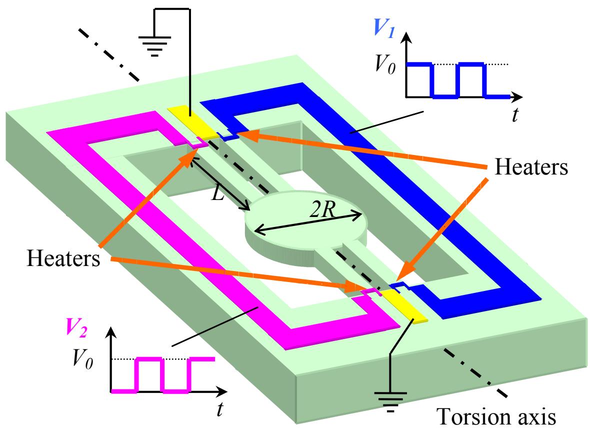

Figure 1: Schematic view of the temperature-gradient driven micromirror. The 1 mm diameter mirror is suspended on four 1200 μm long beams.

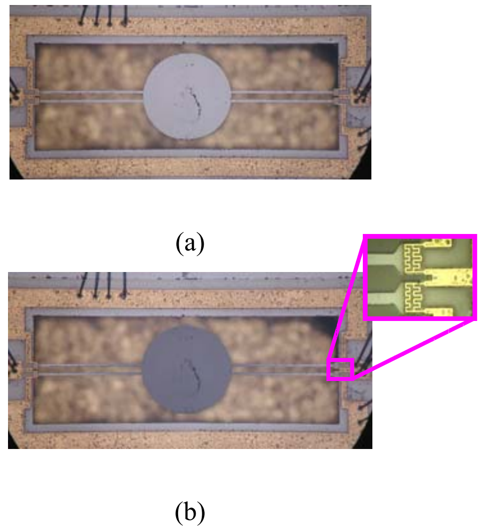

Figure 2: A microphoto of the micromirror device a) before actuation, b) during actuation, with a blow-up of the serpentine shaped heater resistor. When in motion, the mirror appears darker than the anchors.

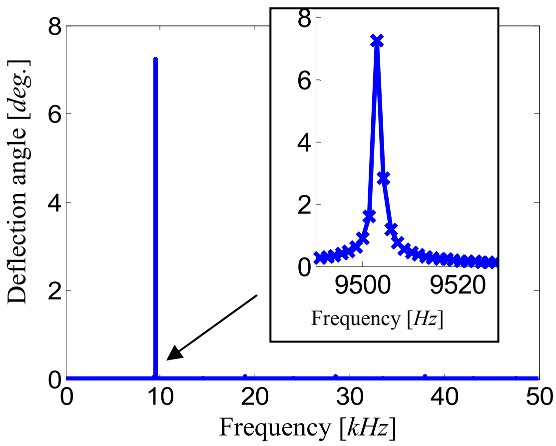

Figure 3: The FFT of the measured deflection angle. This shows that the time response is predominantly sinusoidal.

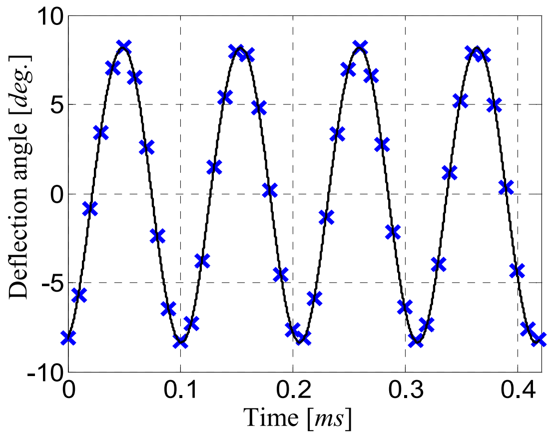

Figure 4: The time response of the micromirror. The marks are the measured points and the solid line is a best fitted sine waveform (least squares).

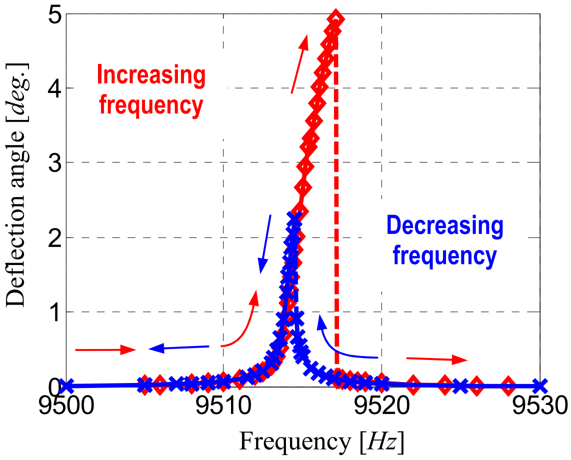

Figure 5: The measured frequency response of the mirror where the amplitude of the applied voltage is V_0=1.1 Volt.

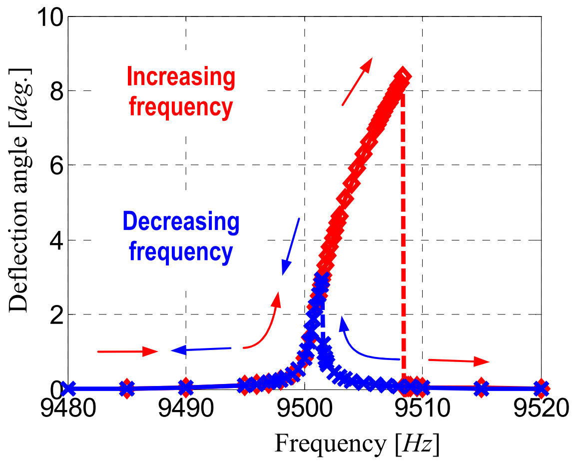

Figure 6: The measured frequency response of the mirror where the amplitude of the applied voltage is V_0=1.5 Volt. The maximal deflection angle is ±8.5° at 9.5 kHz.

Extracting intensity factors for cracked piezoelectric ceramics with various poling directions

Yael Motola*, Lucy Shemesh and Leslie Banks-Sills

The Dreszer Fracture Mechanics Laboratory, Department of Solid Mechanics, Materials and Systems, School of Mechanical Engineering, The Fleischman Faculty of Engineering, Tel Aviv University, Ramat Aviv 69978, Israel. Email: ymotola@eng.tau.ac.il

Piezoelectric ceramics are in widespread use as sensors and actuators in smart structures, despite the absence of a fundamental understanding of their fracture behavior. Piezoelectric ceramics are brittle and susceptible to cracking. As a result of the importance of the reliability of these devices, there has been tremendous interest in studying the fracture and failure behavior of such materials. Deriving accurate numerical methods for extracting intensity factors for cracks in piezoelectric bodies is an important step towards obtaining a better understanding of the fracture behavior of these materials.

Two methods for calculating intensity factors were considered: displacement extrapolation and an area *M*-integral. With the displacement extrapolation method, the intensity factors are found by extrapolation of the displacement along the crack face. Applying this method to piezoelectric materials includes both the displacements and the electric potential, as determined directly from the finite element results. The domain independent *M*-integral is an accurate method for calculating stress intensity factors in mixed modes. Here, the intensity factors are determined indirectly from energy quantities. It should be pointed out that so far, the *M*-integral has not been employed for piezoelectric material.

Based on the approaches of Stroh and Lekhnitskii, the asymptotic expressions for stress, displacement, electric flux density and electric fields have been developed for impermeable boundary conditions, for a crack parallel, perpendicular, at an angle to the poling direction and for a crack front parallel to the poling direction. These asymptotic expressions were used for determining the energy release rates, $\mathsf{G}_I, \mathsf{G}_{II}, \mathsf{G}_{III}$ and G_{IV}.

The numerical investigation included a test problem of a body subjected to essential boundary conditions with a known solution and a benchmark problem of a cracked infinite body subjected to mechanical and electrical loads (also with an exact solution). For the first problem, the displacements were taken as the first term of the asymptotic displacement and electric potential field with constant values for the intensity factors. Hence, the solution in these equations satisfies equilibrium and the constitutive law everywhere within the body. The expected intensity factors are those prescribed on the boundary.

The problems were analyzed by means of the finite element method with the program ANSYS. Eight noded quadrilateral coupled field elements were employed. Quarter-point elements were used at the crack front, so that the square-root singularity was well modeled. In order to calculate the stress distributions at the crack tip, the mesh density was increased near the crack tip. For both methods, namely displacement extrapolation and the area *M*-integral, the numerical errors in the intensity factors were relatively small (less than 2%).

Brittle failure initiation at a V-notch tip under mixed mode loading

Elad Priel* and Zohar Yosibash[1]
Dept. of Mechanical Engineering,
Ben-Gurion Unviersity, Beer-Sheva, Israel.
Email: prielel/zohary@bgu.ac.il

Brittle structural components containing V-notches may fail suddenly at significantly lower loads than the apparent material strength would suggest. Experiments have shown that failure is caused by the initiation of a small crack emanating from the V-notch tip. There are many papers on failures in components having a V-notched tip under *mode I* loading but few address the case of failures under *mixed mode (I and II)* loading. The ones that do address the problem perform a classical asymptotic analysis leading to the conclusion that only the first symmetric load governs the mechanics of crack initiation. This also suggests that the crack starts along the bisector of the v-notch.

Experiments we preformed on PMMA and Alumina specimens using non symmetric 3PB tests contradict this and show that the crack direction is clearly inclined with respect to the bisector. By using finite fracture mechanics it can be shown that an infinitely small crack length is incompatible with the energy balance. In fact, at crack initiation the crack "jumps" a finite distance which is determined by the material failure parameters and by the V-notch geometry. The distance is still small compared to the specimen size but is sufficiently large so that the second mode is no longer negligible. A theoretical difficulty arises from the different singular exponents involved in the first two modes. Nevertheless a complete finite fracture model can be carried out in mixed mode loading with an original approach of the mode mixity. It allows to predict both the critical failure loads and the crack direction at initiation. The new mixed mode failure criterion will be described and its validation by experiments in both symmetric and non symmetric loading will be reported. Both the critical load and crack direction at initiation are well predicted as shown in the figure below.

[1]This work is in collaboration with Prof. D. Leguillon, University Pierre et Marie Curie (Paris 6), France.

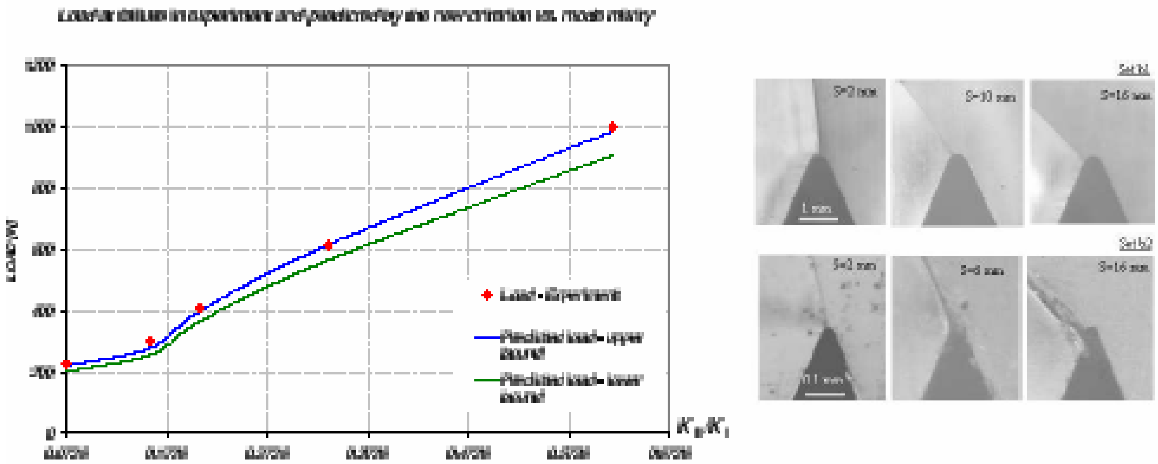

Figure 1: Experimental load at failure and its prediction by the newly proposed failure criterion (Left) and crack direction (right) for different $K_{II} = K_I$ ratios.

Laminated Electro-Active Polymer Composites

Limor Tevet-Deree*, Esteban A. Socolsky and Gal deBotton

Department of Mechanical Engineering, Ben-Gurion University of the Negev
P.O. Box 653, Beer-Sheva 84105, Israel. *Email: tevetl@bgumail.bgu.ac.il

The class of electroactive polymers has been developed to a point where real life applications as "artificial muscles" are conceivable. These actuator materials provide attractive advantages: they are soft, light-weight, undergo large deformations, possess fast response time and are resilient. However, wide-spread application has been hindered by their limitations: the need for large electric field, relatively small forces and energy density. It is now recognized that the limitations arise from poor electro-mechanical coupling in typical polymers. This in turn is related to the fact that the typical polymers have a small ratio of dielectric to elastic modulus (flexible polymers have low dielectric modulus while high dielectric moduli polymers are stiff).

We carry out preliminary calculations for different classes of composites. For the class of sequentially laminated composites explicit expressions relating the electrostatic excitation to the overall mechanical response are derived. These calculations demonstrate that the electromechanical coupling can be improved by considering non-homogeneous electromechanical actuators. In particular, we show that the overall response of a composite actuator can be better than the responses of its constituents. These findings are in agreement with recent experimental work showing that the limitations of these actuators can be overcome by making composites of flexible and high dielectric modulus materials [1].

We also carry out numerical simulations of electroactive fiber composites with periodic hexagonal cells. These calculations are based on finite element simulations by application of ABAQUS. We find that, in a manner resembling the purely mechanical case, the analytical results for the coupled electromechanical problem for the class of sequentially laminated composites are in agreement with the FE simulations for the fiber composites.

Reference:

Huang, C., Zhang, Q. M., deBotton, G. and Bhattacharya, K., "All-organic dielectric percolative three-component composite materials with high electromechanical response", *Applied Physics Letters*, pp.4391-43.

Participants Index